JOURNAL OF PROPULSION AND POWER
Vol. 21, No. 3, May–June 2005

On Flow Development in Jet-Driven Vortex Chambers

Ali Jawarneh,* Georgios H. Vatistas,† and Henry Hong‡
Concordia University, Montreal, Quebec H3G 1M8, Canada

This paper presents a cohesive study of flow in a jet-driven vortex chamber for a wide range of Reynolds numbers, contraction ratios, inlet angles, areas, and aspect ratios. Dimensional analysis furnishes the general functional relationships between the fundamental dimensionless quantities. Application of the integral equations of continuity and energy over the control volume, along with the minimum-pressure-drop or maximum-flow-rate postulate, provide the required analytical means to relate the predominant nondimensional parameters such as the chamber geometry, core size, pressure drop, Reynolds number, and viscous losses. The theoretical results successfully capture most of the salient properties of the flow. A parametric examination explores how the pressure coefficient and the core size vary with the different dimensionless properties. The observations show the pressure drop to decrease with the length. At first this appears to be counterintuitive since one habitually expects the pressure drop to be larger for longer pipes. A closer consideration, however, reveals that in addition to the radial–axial plane flow there is also a substantial centrifugal force, which decays with the length, thus shaping the development of the overall flowfield. Last, the current theory confirms that the previous published models are only applicable for high Reynolds numbers where the inertia dominates the viscous forces.

Nomenclature

A_{in}	=	total inlet area
A_o	=	cross-sectional area of the vortex chamber
C_p	=	pressure coefficient ($2\Delta P/\rho q_{\text{in}}^2$)
D_e	=	diameter of the exit port ($2R_e$)
D_{in}	=	diameter of the inlet port
D_o	=	chamber diameter ($2R_o$)
L	=	chamber length
P	=	static pressure
P_a	=	ambient static pressure
P_{in}	=	static pressure at the inlet
Q	=	volumetric flow rate
q_{in}	=	total velocity vector at the inlet
R_c	=	core radius
R_e	=	radius of exit port
R_o	=	radius of the chamber
r, θ, z	=	radial, tangential and axial coordinate respectively
V_r, V_θ, V_z	=	radial, tangential and axial velocity components
$V_{z\,\text{out}}$	=	axial velocity component at exit
$V_{\theta\text{in}}$	=	inlet tangential velocity component
α	=	area ratio (A_{in}/A_o)
ΔP	=	static pressure difference ($P_{\text{in}} - P_a$)
δ	=	vortex decay factor
ζ	=	aspect ratio (L/D_o)
κ_{in}	=	vortex strength at the inlet ($R_o V_{\theta\text{in}}$)
κ_{out}	=	vortex strength at the outlet ($\delta R_o V_{\theta\text{in}}$)
ξ	=	diameter ratio (D_o/D_e)
ρ	=	density of the fluid
φ	=	angle between the total velocity vector and the tangential velocity component at the inlet (inlet angle)
χ_c	=	dimensionless core size at exit (R_c/R_e)
χ_{co}	=	dimensionless core size (R_c/R_o)

Received 16 February 2004; revision received 14 September 2004; accepted for publication 18 October 2004.

*Research Assistant, Mechanical Engineering Department, 1455 DeMaisonneuve Boulevard West.

†Professor, Mechanical Engineering Department, 1455 DeMaisonneuve Boulevard West. Senior Member AIAA.

‡Assistant Professor, Mechanical Engineering Department, 1455 DeMaisonneuve Boulevard West.

I. Introduction

ADVANTAGEOUS properties of swirling flow in cylindrical confinements have long been put into use in several technological devices and industrial processes. The most notable of them include vortex separators, pumps, gas turbine combustors, incinerators, furnaces, and the swirl atomizer. In the range of intermediate aspect ratios (length/diameter), the vortex separator is one of the most widespread of the applications. The vortex combustor can provide easy ignition, efficient and stable combustion, and low levels of emissions for a wide range of air-to-fuel ratios. In furnaces and incinerators, swirl keeps the solid fuel in suspension, increases its residence time, and compels even the most difficult (low-calorific-value) fuel to burn completely. Energy separation can be achieved in vortex tubes. The vortex valve has been used in fluidics, as a means to prevent floods, and as a flow rate sensor. The supporting effects of swirling fluid motion have also found applications in magnetohydrodynamic power generation and the stabilization of electric arcs. In addition vortex tubes have become the laboratory tool to study the phenomenon of vortex-breakdown phenomenon and to examine the main properties of high-Rossby-number geophysical vortices. The general area is also of value to ion flow dynamics, to low-temperature physics, and to several other related fields. The plethora of journal articles, monographs, and industrial/laboratory reports on the subject have shown this area to be under continuous scientific scrutiny since the late 1940s. As a result, an enormously large number of articles have been written. In order to avoid the production of a review article and limit an otherwise long list of references only the contributions that are pertinent to the present investigation will be cited. For a through review of the subject the reader should consult the fine contributions of Lewellen,[1] Gupta et al.,[2] and Ogawa.[3]

The physics of strong vortex flows, particularly the confined type, are theoretically cumbersome because in addition to the usual forces they also include a powerful centrifugal acceleration and complex boundary conditions (oftentimes unknown), which exacerbate the situation. These complications have prevented analytical or even numerical solutions from being able to capture the physics adequately. For this reason the majority of the theoretical studies have been limited to either simple solutions of the equations of motion or numerical flow descriptions using very approximate exit boundary conditions.

The bulk of experimental work has dealt primarily with specific applications. Consequently, the data are restricted to the geometry and flow conditions of the individual study. The main obstacle to

reliably compare results is the lack of lucid rules with which dynamic similarity among flows can be secured. The experimental studies can be divided into two categories: those directed toward the characterization of the overall flow behavior, concentrating on the pressure drop and flow rate through the device, and those aimed at the elaboration of the internal flow structure. Tests to explain the flow features include visualization, pitot probe, and hot wire, as well as laser doppler anemometer (LDA) measurements. Yet the experimental side of the problem is not free from impediments. Intrusive measuring techniques tend to slow down the vortex, thus altering the flow structure.[4] Visualization, on the other hand, can only be limited to low Reynolds numbers because the tracer particles at high flow rates are prone to diffusion, producing a fuzzy picture of the flow field. Due to centrifugal instability and depending on the flow conditions, vortices are known to host a variety of waves.[5,6] These are generated near the axis of rotation and then are diffused outward. The last action modulates the main flow properties in the vicinity of the axis of rotation, causing temporal variation. Consequently, the location of the vortex center may vary significantly with time. If this is the case, even the LDA data will not provide the actual magnitude of the tangential velocity but rather an averaged value.

Vortex chambers in general have a cylindrical configuration with a centrally located outlet located on the top or the bottom plate. Fluid entering the tube acquires swirl via either 1) inlets placed tangentially around the circumferential wall, 2) rotation of a porous wall, or 3) admission through radial or axial vanes. The inlet(s) may be located near the top plate, the opposite end, or both, or cover the entire length of the chamber. Inlet(s) with both rectangular and circular cross-section(s) have been used in the past. The present paper will focus on jet-driven vortex chambers, case 1).

As the fluid enters the vortex chamber it immediately faces a strong centrifugal force. In its attempt to find paths to the exit with a minimum opposition it divides itself into two streams. The first propagates along the circumferential wall where the centrifugal force is constant, and is then directed to the outlet at a point near the top plate. The second flows toward the center through the bottom plate. In both plates the presence of Ekman's boundary layers reduce the velocity thus diminishing the centrifugal force. Because the path through the top plate the tangential velocity has undergone decay it presents the least centrifugal opposition of the two streams. Consequently the first stream is stronger than the second. A large toroidal recirculation flow area that exists between the exit radius and the cylindrical wall (see Georgantas et al.,[7] Baluev and Troyankin,[8] Escudier et al.[9]) has its origin in Taylor–Göertler instability. However, a recent study by Mattner et al.[10] indicated otherwise. Depending on flow conditions and chamber geometry, the axial velocity near the core could develop a distribution resembling that of a pure jet, a jet-like profile with a velocity deficit at the axis of rotation, or even a wake-like profile. The last flow state is characterized by the development of entrained flow.

One of the important operational characteristics in vortex chambers is the pressure drop. The last has been the subject of a few studies in the past. The early studies of Binnie and Hookings[11] focused on the discharge of water through trumpet-shaped circular weirs. Lewellen[1] utilizes the maximum-flow-rate hypothesis to determine the core size. Shakespeare and Levy[12] reported experimental findings with respect to the pressure drop and the core size in a vortex chamber with a rotating permeable inlet, assuming a potential flow. Their analytical development veers away from the last hypothesis and unfortunately creates a theoretical contradiction. Vatistas et al.[13,14] also used the extremum assumption to analyze the flow inside vortex chambers.

The work to be presented here deals with the main flow properties in chambers having one axial outlet port. Based on dimensional analysis the functional relationships of the main dimensionless groups will be given. The analytical work, which is an extension of previous work by Vatistas et al.[13,14] in single-outlet chambers, provides the formulae that relate the dominant nondimensional parameters. For strongly swirling flows with small inlet angle, the experimental results will be shown to agree reasonably well with the theoretical findings.

II. Experiments

Vortex chambers are in general cylindrical with outlets located on the top plates. A similar type of flow can be accomplished using a rotating chamber with a porous circumferential wall, from which fluid can easily enter into the chamber.

The present experiments have been conducted using a jet-driven vortex chamber that is shown in Fig. 1. The chamber has a constant diameter (5.5 in.), whereas the rest of the geometrical parameters are variable; see Table 1. Swirl is imparted to the fluid via the vortex generator shown in detail in Fig. 1. Its modular design makes the variation of the area ratio (A_{in}/A_o) and the inlet flow angle φ easier. The required sets of inlet conditions are realized by insertion of the appropriate vortex generator blocks (swirlers) into the vortex generator assembly. Along the periphery of the vortex generator block, a number of openings of circular cross section are drilled at a specified angle φ. The static pressure is measured by a series of taps located ahead of the tangential ports and is averaged by connecting in parallel all the pressure pickup tubes into a common tube. The measurements of the mean gauge pressure, $P_{\text{in}} - P_a$, were obtained using a U-tube filled with Meriam oil, having a specific gravity equal to 1.00. A rotameter was used to measure the volumetric flow rate of the inlet air. This was carefully calibrated under standard conditions (1 atmosphere and 0°C). For the flowrates used, the uncertainty was estimated to be from 1.4 to 2.0%.

The geometrical characteristics of the vortex chamber used for the present experiments are given in Table 1. The chamber has a cylindrical shape with constant cross-sectional area. Its length, defined as the distance between the two end plates, was varied. The axis of the vortex chamber was horizontal with respect to the ground, with the

Table 1 Geometrical characteristics of the vortex chamber

φ (deg)	D_{in} (cm)	No. of inlet ports	A_{in} (cm^2)	D_e (cm)	L (cm)
20	0.7874	16	7.787	1.879, 1.976,	
30	1.267	16	20.177	2.164, 2.413,	22, 42,
40	1.905	8	22.79	2.649, 2.794,	83,128,
40	1.905	4	11.395	3.175, 3.81,	164,225
60	1.905	8	22.79	4.191, 5.588	

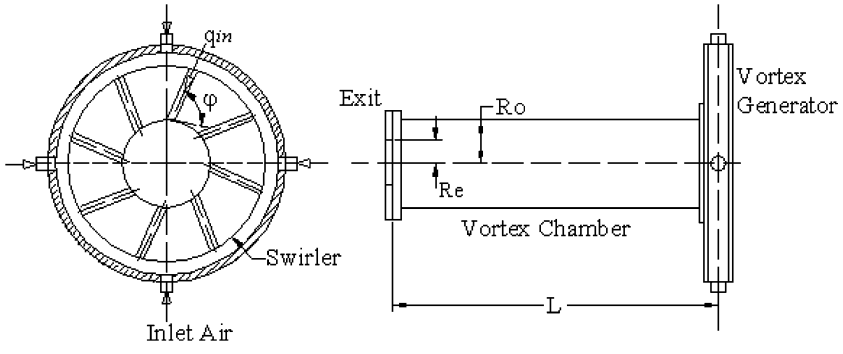

Fig. 1 Schematic of the vortex chamber.

swirler placed opposite to the outlet plate. The design of the swirler was made in a way that the total inlet area did not change with the inlet angle φ. Air at standard temperature was the working fluid. A typical experimental run involved the following simple routine. A specific size outlet was fixed onto the end of the chamber. The flow rate was set at at a specific flow rate and the static pressure was recorded using the manometers mentioned earlier.

III. Analysis

A complete theoretical study of this flow requires a differential characterization of the internal flow through the solution of the Navier–Stokes and continuity equations. Quite often, however, an adequate description can be achieved by concentrating on the overall features (integral approach) and thus avoiding the particulars of the interior flow. The present research will use the second method.

Consider the steady, incompressible, swirling flow within the vortex chamber of Fig. 2. Experiments have shown the pressure drop across the vortex chamber ($\Delta P = P_{\text{in}} - P_a$) to depend on the vortex strengths at the inlet (κ_{in}) and outlet (κ_{out}), the flow rate (Q), the inlet area (A_{in}), the length of the chamber (L), its radius (R_o), the radius of the outlet (R_e), the vortex core radius (R_c), and the fluid density (ρ) and its viscosity (μ), or

$$P_{\text{in}} - P_a = \text{fn}(\kappa_{\text{in}}, \kappa_{\text{out}}, L, R_o, R_e, R_c, A_{\text{in}}, Q, \rho, \mu)$$

Therefore, because there are 11 variables and 3 basic dimensions involved with the problem, the same phenomenon must be equivalently described by the 8 dimensionless parameters,

$$\Delta\Pi = \text{fn}(\chi, \xi, \varphi, \zeta, \alpha, \delta, R_{\text{eo}})$$

where

$$\Delta\Pi = \frac{2(P_{\text{in}} - P_a)}{\rho q_{\text{in}}^2}, \qquad \chi = \frac{R_c}{R_e}, \qquad \xi = \frac{R_o}{R_e}$$

$$\varphi = \cos^{-1}\left(\frac{V_{\theta\text{in}}}{q_{\text{in}}}\right), \qquad \zeta = \frac{L}{D_o}, \qquad \alpha = \frac{A_{\text{in}}}{A_o}, \qquad \delta = \frac{\kappa_{\text{out}}}{\kappa_{\text{in}}}$$

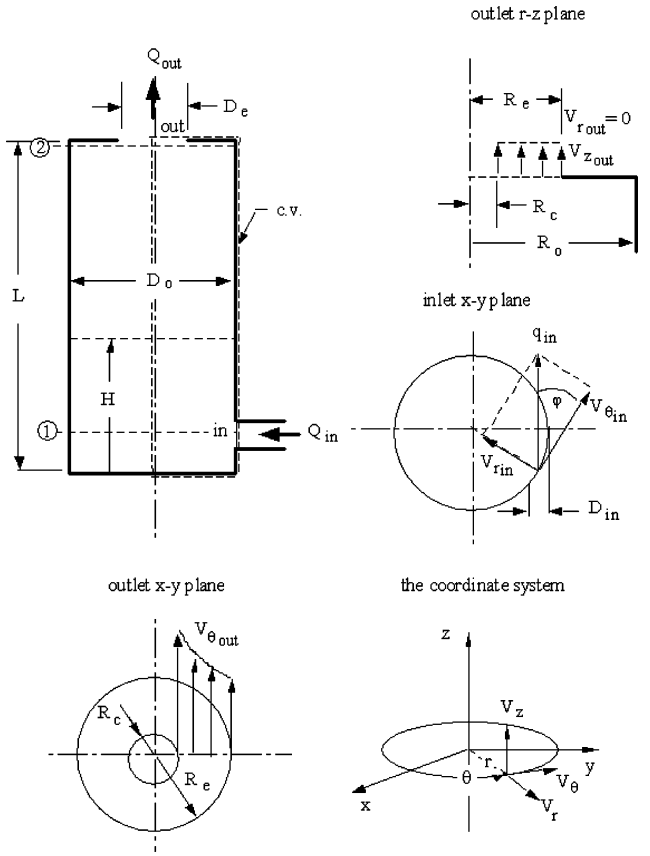

Fig. 2 Schematic of the problem.

and the Reynolds number (R_{eo}) based on the average axial velocity, defined as

$$R_{\text{eo}} = 4Q/\nu\pi D_o$$

The above analysis furnishes the expected functional relations among the main dimensionless parameters associated with the problem.

Under these assumptions, the energy equation over the control volume is given by

$$\oint_{\text{c.s.}} \left(\frac{P}{\rho} + \frac{1}{2}\boldsymbol{q}^2\right)\boldsymbol{q} \circ \boldsymbol{n}\, \mathrm{d}A + F = 0 \tag{1}$$

where F is the loss due to vortex decay. Furthermore, the flow field is assumed to be axisymmetric, the radial velocity component at the exit is considered to be negligibly small in comparison to the other two, whereas the total inlet velocity and static pressure are both uniform, and the exit pressure is equal to the ambient; thus Eq. (1) simplifies into

$$\left(\frac{P_{\text{in}}}{\rho} + \frac{1}{2}q_{\text{in}}^2\right)Q = P_a \int_{R_c}^{R_e} V_{z\,\text{out}} 2\pi r\, \mathrm{d}r + \int_{R_c}^{R_e} \frac{1}{2}\left(V_{\varphi\,\text{out}}^2 + V_{z\,\text{out}}^2\right)V_{z\,\text{out}} 2\pi r\, \mathrm{d}r + F \tag{2}$$

In order to evaluate the integrals in Eq. (2), the variations of both tangential and axial velocity components as a function of the radius must be provided. Based on the work of Vatistas et al.[13] the axial velocity at the exit is regarded as uniform:

$$V_{z\,\text{out}} = Q\big/\pi\left[R_e^2 - R_c^2\right]$$

whereas the tangential velocity is given, as in a free vortex, by

$$V_{\varphi\,\text{out}} = \delta\kappa_{\text{in}}/r$$

where $Q = q_{\text{in}}A_{\text{in}}$, $\kappa_{\text{in}} = V_{\varphi\,\text{in}}R_o$, and $V_{\varphi\,\text{in}} = q_{\text{in}}\cos(\varphi)$.

The anticipated diminishing strength of the tangential velocity evident from the LDA results of Yan et al.[15] is mathematically denoted by the factor δ, which takes on values between zero and one.

Energy losses F can be taken into account if the detailed flow field inside the chamber is known. Because the latter is currently not available, an attempt will be made here to include it through the reduction of the swirl kinetic energy between planes 1 and 2 (see Fig. 2),

$$F = \frac{\Delta k \cdot e_{\theta 1\to 2}}{\rho} = \frac{1}{2}\int_{R_c}^{R_o}\left(V_{\varphi 1}^2 - V_{\varphi 2}^2\right)V_{zo} 2\pi r\, \mathrm{d}r$$

where

$$V_{\varphi 1}^2 - V_{\varphi 2}^2 = (1-\delta^2)V_{\varphi 1}^2 = (1-\delta^2)(\kappa_{\text{in}}/r)^2$$

and

$$V_{zo} = Q\big/\pi\left(R_o^2 - R_c^2\right)$$

In view of the above-mentioned simplifications, Eq. (2) reduces to

$$\Delta P = P_{\text{in}} - P_a = \left(\rho C_p\big/2A_{\text{in}}^2\right)Q^2 \tag{3}$$

where

$$C_p = \frac{\alpha^2\xi^4}{(1-\chi^2)^2} - 2\frac{\delta^2\xi^2\cos^2(\varphi)\,\ell_n(\chi)}{(1-\chi^2)} - 2\frac{(1-\delta^2)\cos^2(\varphi)\,\ell_n(\chi/\xi)}{1-(\chi/\xi)^2} - 1 \tag{4}$$

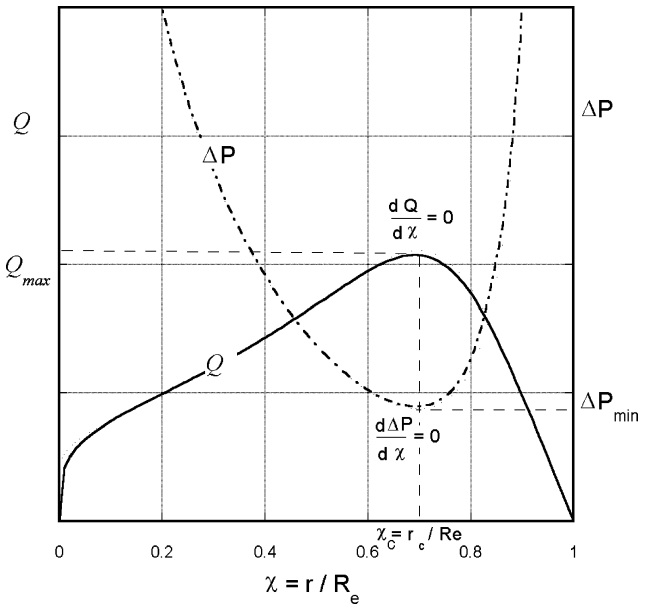

Fig. 3 The extremum condition.

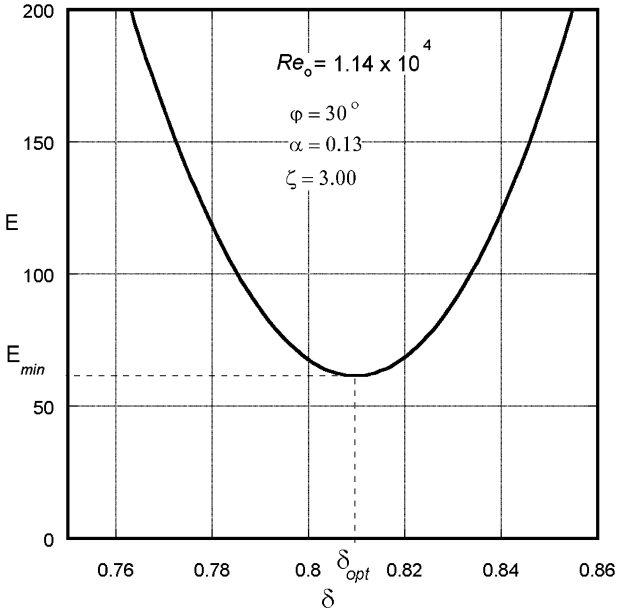

Fig. 4 The minimum squared error criteria.

Given that the geometry of the chamber and δ are fixed, taking the derivative of Eq. (3) with respect to χ, results in

$$\frac{\mathrm{d}\Delta P}{\mathrm{d}\chi} = \frac{\rho}{A_{\mathrm{in}}}\left(C_p Q\frac{\mathrm{d}Q}{\mathrm{d}\chi} + \frac{Q^2}{2}\frac{\mathrm{d}C_p}{\mathrm{d}\chi}\right) \tag{5}$$

For a given flowrate Q the above equation yields

$$\frac{\mathrm{d}\Delta P}{\mathrm{d}\chi} = \frac{\rho}{A_{\mathrm{in}}^2}\frac{Q^2}{2}\frac{\mathrm{d}C_p}{\mathrm{d}\chi}$$

If now one fixes ΔP, Eq. (5) gives

$$\frac{\mathrm{d}Q}{\mathrm{d}\chi} = -\frac{Q}{2C_p}\frac{\mathrm{d}C_p}{\mathrm{d}\chi}$$

At the extreme, for $\chi = 0$ and 1, ΔP will be unbounded, whereas Q will be zero. Between these values of χ, there is a critical value χ_c where ΔP and Q attain extrema, an absolute minimum for the former and an absolute maximum for the latter; see Fig. 3. Therefore, the last principle can be used, as the supplementary condition required for the determination of the vortex core size. Binnie and Hookins[11] first introduced the previous postulate in their investigations with regard to the discharge of swirling flow through trumpet-shaped circular weirs. A similar approach was also taken by Lewellen[1] and Vatistas et al.[13] in their analysis of vortex flows confined in tubes.

The static pressure drop in dimensionless form is

$$\Delta\Pi = 2\Delta P \big/ \rho q_{\mathrm{in}}^2 = C_p$$

The minimum $\Delta\Pi$ principle yields

$$\Big(2a_1\chi^2 - a_2\{1-\chi^2\}\{\chi^2[2\,\ell_n(x)-1]+1\}\Big)[1-(\chi/\xi)^2]$$
$$+\,a_3(1-\chi^2)^3\{1-[\chi/\xi]^2[2\,\ell_n(\chi/\xi)-1]\} = 0 \tag{6}$$

where

$$a_1 = \alpha^2\xi^4, \qquad a_2 = \delta^2\xi^2\cos^2(\varphi), \qquad a_3 = (1-\delta^2)\cos^2(\varphi)$$

Given the values of α, φ, ξ, and δ the above equation can be solved numerically for χ using any of the traditional root-finding methods. In order to know the value of δ one must know how the vortex decays. Because the last is not available its value will be found based on the experimental results using a modified version of the least-squares technique.

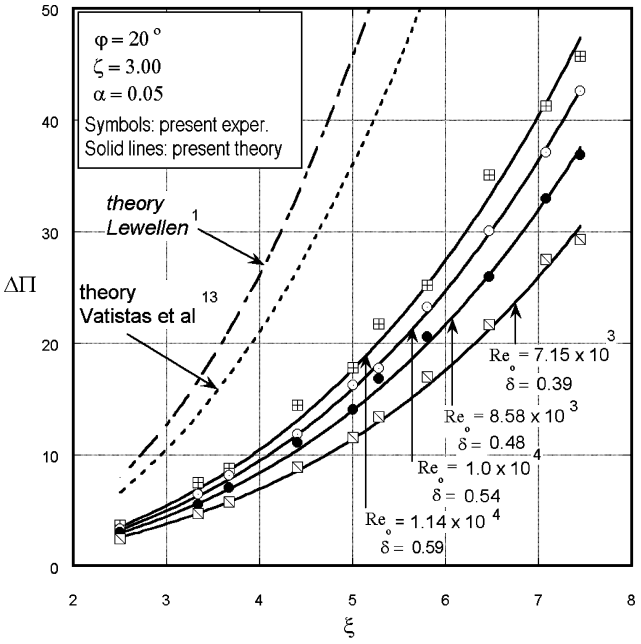

Fig. 5 Pressure drop in an intermediate-aspect-ratio chamber for a small inlet angle for different Reynolds numbers.

The observations will provide the data on $\Delta\Pi$ across a vortex chamber operating under specific conditions. The above theory will then be applied to curve-fit the results assuming values of δ and calculating the squared error according to the formula

$$E = \sum_{i=1}^{N}(\Delta\Pi_{\mathrm{exp}\,i} - \Delta\Pi_{\mathrm{theo}\,i})^2$$

The last will generate a graph such as the one shown in Fig. 4. The optimum δ for a given set of data will then be the one that produces the least squared error (E).

IV. Analysis of Results

First, consider the pressure drop across a chamber with configuration $\varphi = 20$ deg, $\alpha = 0.05$, $\zeta = 3.00$, where the flow field is expected to be under intense swirl conditions. The results for this case are shown in Fig. 5. A good correlation between the present theory

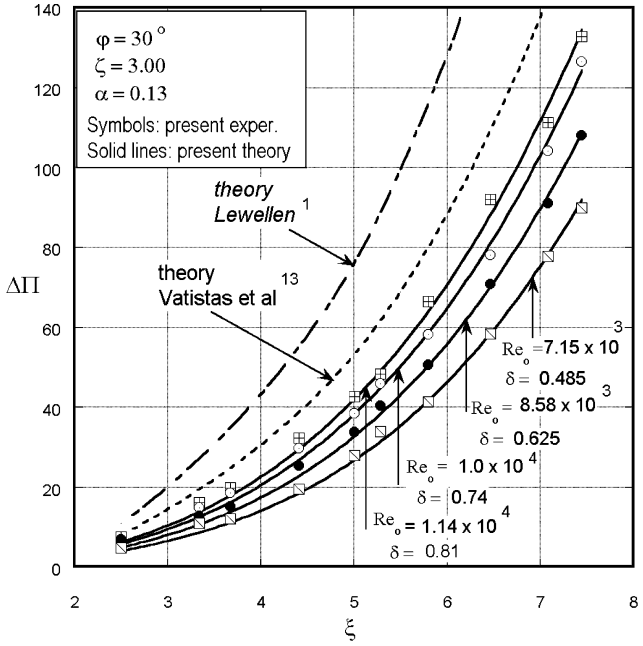

Fig. 6 Pressure drop in an intermediate-aspect-ratio chamber and inlet angle for different Reynolds numbers.

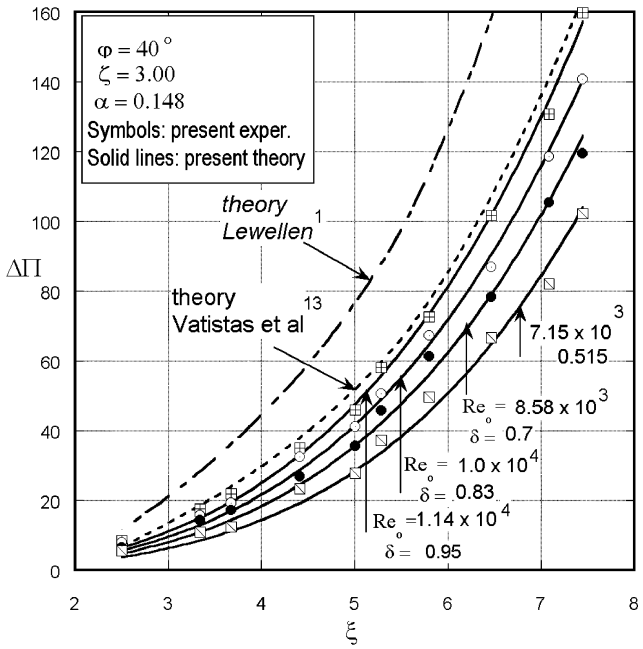

Fig. 7 Pressure drop in an intermediate-aspect-ratio chamber for a large inlet angle for different Reynolds numbers.

and experiment is evident as the maximum difference between the theory and the experiment is less than 10%. A similar level of correlation is also the case for the configurations $\varphi = 30$ deg, $\alpha = 0.131$, $\zeta = 3.00$, and $\varphi = 40$ deg, $\alpha = 0.148$, $\zeta = 3.00$, when ξ is larger than, say, 5 and 6, respectively; see Figs. 6 and 7. For all three cases the conformity of the analytical result to the observations is better in the region of high ξ values.

The LDA experiments of Yan et al.[15] have shown that the core size inside the chamber stays nearly constant along the height. Assuming that the core at the exit plane is the same as that inside the chamber, the present theory is employed next to predict the core size and compare it with the observed values. The results are shown in Fig. 8, where an acceptable correlation between the two is apparent. In this case the experimental $\chi_{co}(\chi_c R_e/R_o)$ values have been ascertained by fitting the Vatistas et al. $n = 2$ vortex model[16] to the LDA

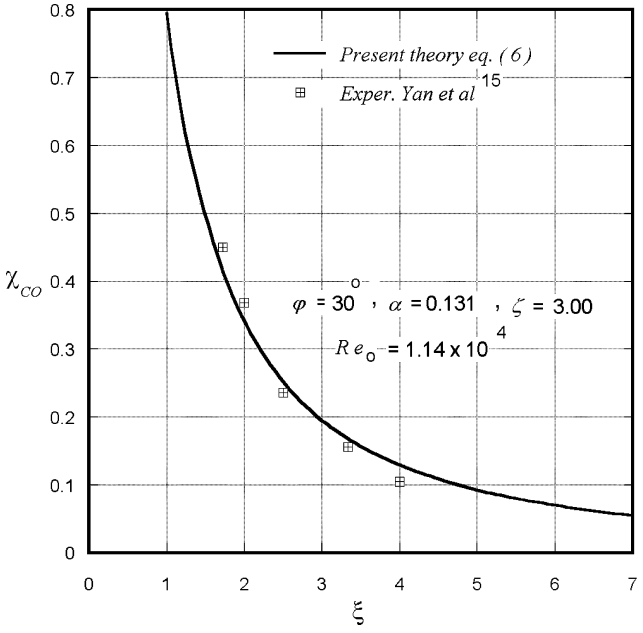

Fig. 8 Core size variation.

velocity data using the least-squares method with one of the unknown variables being the core size, whereas the other is the vortex strength.

Any of Figs. 5, 6, and 7 point out that δ increases with R_{eo} tending toward one for larger R_{eo} values. The last makes the pressure profiles approach the formulation of Vatistas et al.,[13] which assumes $\delta = 1.00$. This propensity is amply evident for configuration $\varphi = 40°$, $\alpha = 0.148$, $\zeta = 3.00$; see Fig. 7, where the pressure coefficient is seen to come within the reach of Vatistas et al.[13] The preceding does not, however, imply that friction is less for higher R_{eo} numbers but rather that under these conditions the inertia being considerably larger overshadows the viscous effects. After all, this is precisely the definition of the Reynolds number. Hence the theoretical development of Refs. 1 and 13 must be limited to the high-Reynolds-number region where the inertia dominates and ignoring friction (one of their main assumptions) will not produce large discrepancies. This by no means suggests that the present development is free of limitations. Because the frictional losses due to the *secondary flow*, taking place in the r–z plane have not been considered, discrepancies in the flow regime where these are no longer insignificant are anticipated. The regime where the last may be substantial is for $\xi < 6$ ($\varphi = 40$ deg, $\alpha = 0.148$, $\zeta = 3.00$) where a maximum of 32% difference between the theoretical and experimental pressure drop was observed.

Having demonstrated that the present theoretical formulation can reasonably correlate the pressure drop in a vortex chamber, we are proceeding now to examine analytically a number of flow features. The pressure drop is made up from the axial inertial term,

$$\mathrm{In} = \alpha^2 \xi^4 / (1 - \chi^2)^2$$

the swirl term,

$$\mathrm{Sw} = -2 \frac{\delta^2 \xi^2 \cos^2(\varphi)\, \ell n(\chi)}{(1 - \chi^2)}$$

and the friction term,

$$F = -2 \frac{(1 - \delta^2) \cos^2(\varphi)\, \ell n(\chi/\xi)}{1 - (\chi/\xi)^2}$$

It is apparent from Fig. 9 that as ξ increases and in order to minimize the pressure drop across the chamber, the vortex core χ_c decreases, but the effective outlet area σ,

$$\sigma = A_e/A_o = \left(1 - \chi_c^2\right) \Big/ \xi_c^2$$

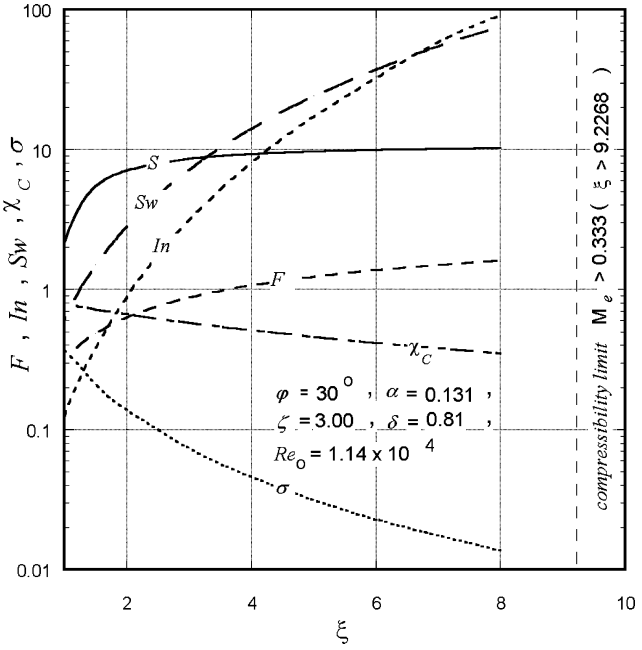

Fig. 9 Variation of the various flow components in a typical chamber.

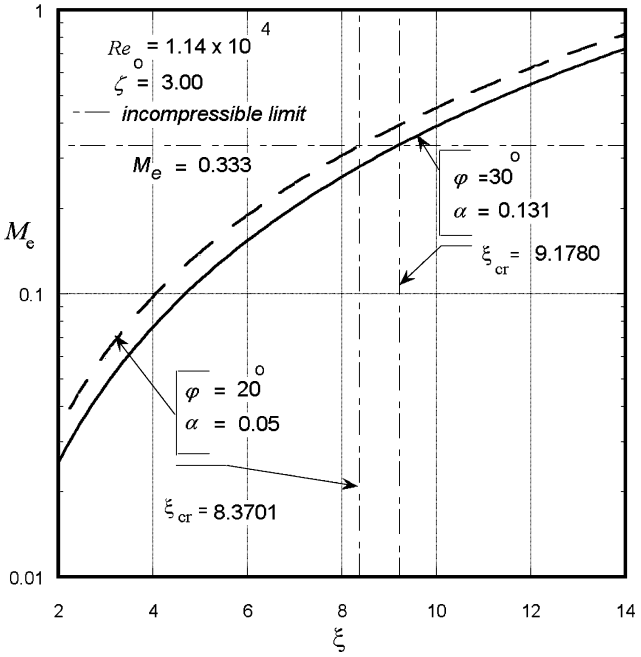

Fig. 10 Compressibility limits.

contracts, giving rise to the increase of inertia term. Since the core always occurs between $0 < \chi_c < 1.0$, as ξ becomes larger the vortex is focused, the swirl term increases, and the frictional effects rise also. For $\xi < 1.5$ (large exit port diameter) the F term is significant, whereas the In is negligibly small in comparison to the other two. For $\xi > 1.5$ the In term begins to overtake friction, whereas for $\xi > \sim 6.8$ it surpasses even Sw.

Traditionally the degree of swirl in a given flow field is expressed by the *swirl number* S, which is defined in Gupta et al.[2] as

$$S = G_{\theta o}/G_{zo}$$

where $G_{\theta o}$ is the momentum flux in the θ-direction,

$$G_{\theta o} = \int_{R_c}^{R_o} \rho V_{\theta o} V_{zo} 2\pi r \, \mathrm{d}r$$

G_{zo} is the momentum flux in the z-direction,

$$G_{zo} = \int_{R_c}^{R_o} \rho V_{zo}^2 2\pi r \, \mathrm{d}r$$

Therefore in our situation the swirl number is given by

$$S = [2\delta \cos(\varphi)/\alpha](1 - \chi_c/\xi)$$

For the first configuration, where swirl is the strongest, the current analytical development is applicable for the full set of data. The previously mentioned good correlation between the theory and the experiment is achieved for larger values of S (say 10).

It is evident that for large ξ ratios the agreement of the theoretical pressure with the experiment becomes better. However, given the chamber geometry and flow conditions, the compressibility effect when

$$M_e = \frac{V_{z\,\mathrm{out}}}{\sqrt{\gamma RT}} = \frac{Q\xi^2}{A_o\sqrt{\gamma RT}\left(1 - \chi_c^2\right)} < 0.333$$

provides an upper limit for ξ beyond which the present theory is not applicable since density variations have not been taken into account. The variation of the exit Mach number for the two configurations $\varphi = 20$ deg, $\alpha = 0.05$, $\zeta = 3.00$ and $\varphi = 30$ deg, $\alpha = 0.131$, $\zeta = 3.00$ as a function of ξ is given in Fig. 10. As anticipated, the compressibility limit for $\varphi = 20$ deg, ξ_{cr}, because the swirl effects are

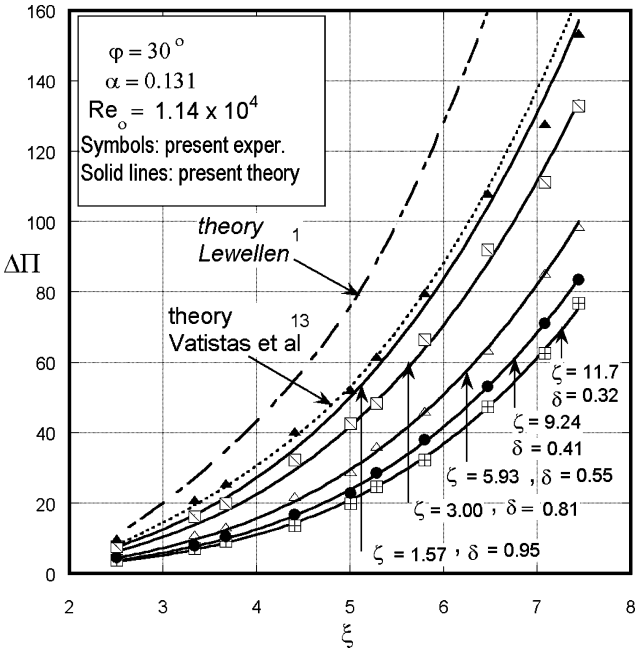

Fig. 11 Pressure drop for an intermediate inlet angle for different lengths.

stronger, forcing the exit area to contract, moves toward the lower values.

The pressure coefficient for various aspect ratios for a chamber with configuration $\varphi = 30$ deg, $\alpha = 0.131$, is given in Fig. 11. The analysis suggests that δ becomes smaller as ζ increases, producing a weaker vortex at the exit plane for longer chambers. If P_a remains constant it means that P_{in} must be decreasing. At first the last appears to be counterintuitive, because one expects the pressure drop to increase as the length is increased. However, here, in addition to the r–z flow, the centrifugal force must also be accounted for, which influences the flow considerably.

In addition to the previously mentioned variables, the pressure drop also depends on the area ratio α. In order to examine the last, half of the inlets were blocked for the configuration $\varphi = 40$ deg, $\alpha = 0.148$, $\zeta = 3.00$ and ΔP was measured. The results are shown in Fig. 12. For the smaller α, the pressure coefficient (C_p) was seen to

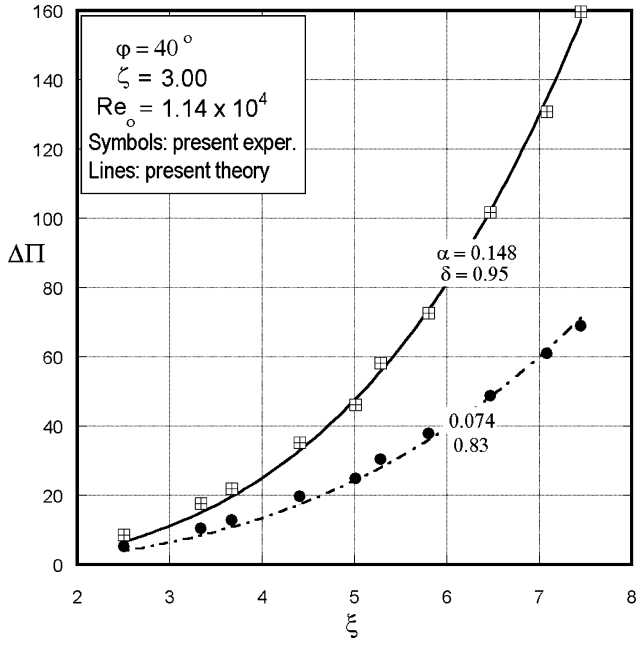

Fig. 12 Pressure drop in an intermediate-aspect-ratio chamber for large inlet angles for different inlet areas.

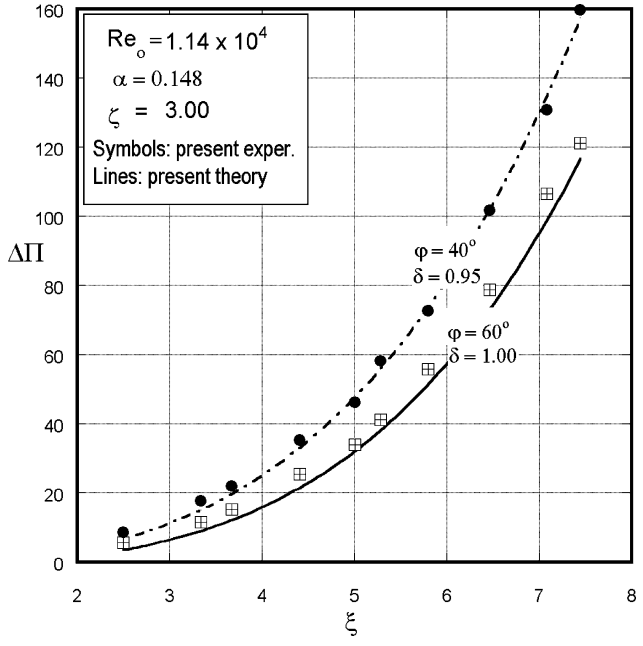

Fig. 13 Pressure drop in an intermediate-aspect-ratio chamber for different inlet angles.

drop, the actual pressure difference (ΔP) increased, and the friction (F) rose.

All the vortex chamber configurations used up to this point have different αs and therefore it is unsuitable to discuss the influence of the inlet angle on the flow development because two variables will be changing at the same time. However, the swirler with $\varphi = 60$ deg has exactly the same α value as that of 40 deg. The results of the study are shown in Fig. 13. It is expected that a stronger vortex is produced for smaller inlet angle and thus the pressure drop for small φs must be large. The latter is amply evident from the same figure.

V. Conclusions

The flow in jet-driven vortex chambers over a wide range of Reynolds numbers, contraction ratios, inlet angles, areas, and aspect ratios was carefully examined. The theoretical tool to investigate the flow analytically was based on the integral equations of continuity and energy, along with the minimum-pressure-drop postulate. When swirl is strong, the formulation has been found to successfully capture the main characteristics of vortex chamber flow. A parametric study gave the details of how the core size and the pressure coefficient change with each of the dimensionless groups. For longer chambers the present analysis suggests that latter flow property is smaller than for shorter chambers. The present investigations have shown of this peculiar flow behavior to the controlling nature of the centrifugal force. The current theoretical development has also shown the previous models to be applicable only to high Reynolds numbers where the inertia dominates the viscous forces.

References

[1]Lewellen, W. S., "A Review of Confined Vortex Flows," NASA CR-1772, July 1971.

[2]Gupta, A. K., Lilley, D. G., and Syred, N., "Swirl Flows," Abacus Press, Tunbridge Wells, England, U.K., 1984.

[3]Ogawa, A., "Vortex Flows," CRC Press, Boca Raton, FL, 1993.

[4]Volchov, E. P., Lebedev, V. P., and Lukashov, V. V., "The LDA Study of Flow Gas-Dynamics in a Vortex Chamber," *International Journal of Heat and Mass Transfer*, Vol. 47, No. 1, Jan. 2004, pp. 35–42.

[5]Thomson, W. [Lord Kelvin], Vibrations of a vortex column. *Philosophical Magazine*, Vol. 10, 1880, p. 155; also A Treatise on Bessel Functions and Their Applications to Physics, edited by A. Gray and G. B. Mathews, Macmillan, London, 1922.

[6]Vatistas, G. H., 1990, A note on liquid vortex sloshing and Kelvin's equilibria, *Journal of Fluid Mechanics*, Vol. 217, Aug. 1990, pp. 241–248.

[7]Georgantas, A. I., Krepec, T., and Kwok, C. K., "Vortex Flow Patterns in a Cylindrical Chamber," AIAA Paper 86-1098, May 1986.

[8]Baluev, E. D., and Troyankin, Y. V., "Study of the Aerodynamic Structure of Gas Flow in a Cyclone," *Thermal Engineering*, Vol. 14, No. 7, 1967, pp. 84–87.

[9]Escudier, M. P., Bornstein, J., and Maxworthy, T., "The Dynamics of Confined Vortices," *Proceedings of the Royal Society of London Series A*, Mathematical and Physical Sciences, Vol. 382, No. 1783, Aug. 1982, pp. 335–360.

[10]Mattner, T. W., Joubert, P. N., and Chong, M. S., "Vortical Flow. Part 1. Flow Through a Constant Diameter Pipe," *Journal of Fluid Mechanics*, Vol. 463, 2002, pp. 259–291.

[11]Binnie, A. M., and Hookings, G. A., "Laboratory Experiments on Whirlpools," *Proceedings of the Royal Society of London, Series A*, Vol. 194, 1948, pp. 398–415.

[12]Shakespeare, W. J., and Levy, E. K., "Pressure Drop in a Confined Vortex with High Flow Rate," *Proceedings of the Winter Annual Conference of ASME*, Chicago, Nov. 1980.

[13]Vatistas, G. H., Lin, S., and Kwok, C. K., "Theoretical and Experimental Studies on Vortex Chamber Flows," *AIAA Journal*, Vol. 24, No. 4, 1986, pp. 635–642.

[14]Vatistas, G. H., Lam, C., and Lin, S., "Similarity Relationship for the Core Radius and the Pressure Drop in Vortex Chambers," *Canadian Journal of Chemical Engineering*, Vol. 67, No. 4, Aug. 1989, pp. 540–544.

[15]Yan, L., Vatistas, G. H., and Lin, S., "Experimental Studies on Turbulence Kinetic Energy in Confined Vortex Flows," *Journal of Thermal Science*, Vol. 9, No. 1, March 2000, pp. 10–22.

[16]Vatistas, G. H., Kozel, V., and Minh, W., "A Simpler Model for Concentrated Vortices," *Experiments in Fluids*, Vol. 11, No. 1, April 1991, pp. 73–76.